Supplemental Materials for - Stable Dirac semi-metal in the allotrope of IV elements

Wendong Cao[1†], Peizhe Tang[2†*], Shou-Cheng Zhang[2], Wenhui Duan[1,3,4**] & Angel Rubio[5,6***]

[1] State Key Laboratory of Low-Dimensional Quantum Physics, Department of Physics, Tsinghua University, Beijing 100084, People's Republic of China;

[2] Department of Physics, McCullough Building, Stanford University, Stanford, California 94305-4045, USA;

[3] Institute for Advanced Study, Tsinghua University, Beijing 100084, People's Republic of China;

[4] Collaborative Innovation Center of Quantum Matter, Beijing 100084, People's Republic of China;

[5] Max Planck Institute for the Structure and Dynamics of Matter and Center for Free-Electron Laser Science, Luruper Chaussee 149, 22761 Hamburg, Germany;

[6] Nano-Bio Spectroscopy group, Dpto. Física de Materiales, Universidad del País Vasco, Centro de Física de Materiales CSIC-UPV/EHU-MPC and DIPC, Av. Tolosa 72, E-20018 San Sebastián, Spain.

[†] These authors contributed equally to this work.

[*] e-mail: peizhet@stanford.edu

[**] e-mail: dwh@phys.tsinghua.edu.cn

[***] e-mail: angel.rubio@ehu.es

SUPPLEMENTARY NOTE 1 - EFFECTIVE $k \cdot p$ MODEL

The Dirac points are the crossing points of two doubly degenerate bands with different $|J_z|$ ($|J_z| = \frac{1}{2}, \frac{3}{2}$). Thus, a 4×4 Hamiltonian model is necessary to describe such a symmetry-protected crossing. The basis states are $\{|J_z, P\rangle\}$ (in the order of $|\frac{1}{2}, -\rangle$, $|\frac{3}{2}, +\rangle$,$|-\frac{1}{2}, -\rangle$,$|-\frac{3}{2}, +\rangle$) , where P labels the odd/even $(-/+)$ partiy. With those basis states and symmetry constraint, the effective Hamiltonian for germancite and stancite is

$$H(\mathbf{k}) = \epsilon_0(\mathbf{k}) + \begin{pmatrix} M(\mathbf{k}) & Ak_+ & 0 & B^*(\mathbf{k}) \\ Ak_- & -M(\mathbf{k}) & B^*(\mathbf{k}) & 0 \\ 0 & B(\mathbf{k}) & M(\mathbf{k}) & -Ak_- \\ B(\mathbf{k}) & 0 & -Ak_+ & -M(\mathbf{k}) \end{pmatrix} \tag{S1}$$

where $\epsilon_0(\mathbf{k}) = C_0 + C_1 k_z^2 + C_2(k_x^2 + k_y^2)$, $k_\pm = k_x \pm ik_y$, $M(\mathbf{k}) = M_0 + M_1 k_z^2 + M_2(k_x^2 + k_y^2)$ and $B(\mathbf{k}) = B_3 k_z k_+^2$. The effective model closely resembles those of Na_3Bi and Cd_3As_2. And the similarity may result from the fact that all those four materials belong to the same classification of Dirac semi-metal in Ref. [1].

The model above is used to fit the calculated electronic structure of germancite and stancite in Fig. 2 (a) (k^3 terms are neglected) and the results are listed in the following table

Material	C_0 (eV)	C_1 (eVÅ^2)	C_2 (eVÅ^2)	M_0 (eV)	M_1 (eVÅ^2)	M_2 (eVÅ^2)	A (eVÅ)
Germancite	2.08	4.88	222	-0.0665	13.4	184	6.27
Stancite	2.08	0.134	35.6	-0.210	0.922	40.5	3.65

Supplementary Table S1. $k \cdot p$ **model fitting parameters for Germancite and Stancite.**

It can be seen that $M_0 \cdot M_1$ and $M_0 \cdot M_2$ are negative in both materials, confirming the band inversion at the Γ point.

SUPPLEMENTARY NOTE 2 - MANIFESTATION OF THE NONTRIVIAL TOPOLOGY OF GERMANCITE (111) FILMS

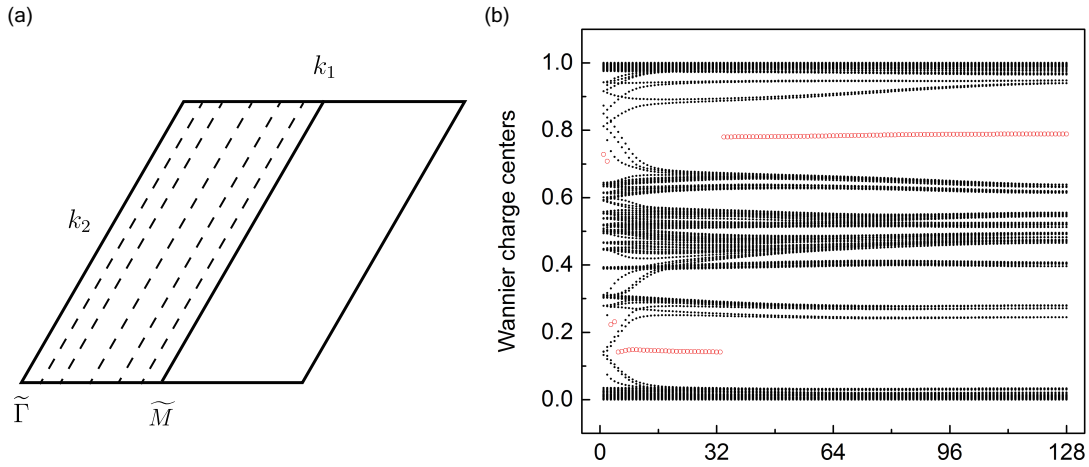

Supplementary Figure S1. **Calculations of $\mathbb{Z}_2$ index.** (a) The first Brillouin zone of Germancite (111) films. There are two momentum directions: k_1 and k_2. And the dashed lines schematically show the integrations along the k_2 direction for each point along the $\widetilde{\Gamma}$-$\widetilde{M}$ line. (b) Evolution of WCCs of 16 layer Germancite (111) film vs k_1. Red dot marks the midpoint of the largest gap. k_1 is sampled in 127 increments from 0 to π along Γ-M.

Even though the inversion symmetry is preserved here, Fu and Kane's method[2] cannot be used to calculate the topological properties because the parity of the basis functions (wannier functions) are unknown. Following the method in Ref. [3], we calculate the evolution of 1D WCCs in half of the 1st Brillouin zone:

$$\bar{x}_n(k_1) = \frac{i}{2\pi}\int_0^{2\pi} dk_2 \langle u_{n\vec{k}}|\partial_{k_2}|u_{n\vec{k}}\rangle \tag{S2}$$

where $|u_{n\vec{k}}\rangle$ is the periodical part of the corresponding Bloch eigenstate with the occupied band index n and momentum $\vec{k}$. The Bloch eigenstate is constructed from the Wannier functions and the integration is along the k_2 direction [see Fig. S1 (a)]. As k_1 increases from 0 to π, the number of WCCs that the gap center jumps over is 169, which is odd [see Fig. S1 (b)]. So the topological index $\mathbb{Z}_2$ is 1 and the 2D Ge film in this new phase is a quantum spin Hall (QSH) insulator.

SUPPLEMENTARY NOTE 3 - STABILITY ANALYSIS

The mass density of germancite (4.58 g/cm^3) is lower than that of germanium in the diamond structure (5.03 g/cm^3). The reason may be that the dumbbell structure distorts the sp^3 hybridization and the lower density is also consistent with the smaller bonding strength, which lowers the energy level s^- at the Γ point and leads to the band inversion. Comparing with other known experimental and theoretical structures, germancite possesses a similar cohesive energy (0.16 eV per Ge atom) under ambient conditions, as shown in the table below. The calculated cohesive energy of germanium in the diamond structure (α-Ge) is set to be zero. Especially, germanium has a cage structure between adjacent layers, similar to another low-density structure Clathrate-II[4]. It may be possible to synthesize germanium by applying the same method and removing the cations of certain Zintl phase (such as Na_mGe_n).

Structure	α-Ge	Clathrate-II[4]	4H[5]	R8[6]	T12[7]	ST12[8]	BC8[9]	β-Sn
Cohesive energy (eV/atom)	0	0.022	0.006	0.139	0.033	0.136	0.134	0.214

Supplementary Table S2. **Comparison of the cohesive energies between germancite and other allotropes of germanium.**

Similarly, the mass density of stancite (4.98 g/cm^3) is lower than that of tin in the diamond structure (5.42 g/cm^3). The calculated cohesive energy of stancite is about 0.12 eV per Sn atom smaller than that of tin in the diamond structure.

SUPPLEMENTARY NOTE 4 - QSH INSULATOR IN GERMANCITE (111) FILMS

For the germancite (111) film, the momentum along the z direction k_z is quantized to be $n\pi/d$, where d is the thickness. After substituting k_z with $n\pi/d$ in Eq. [S1], we find out that the effective model for the germancite (111) film $H_d(k_\parallel)$ equals to the direct sum of $H_{n,d}(k_\parallel)$[10] :

$$H_d(k_\parallel) = \oplus_n H_{n,d}(k_\parallel), \quad H_{n,d}(k_\parallel) = \widetilde{\epsilon}_0(n,k_\parallel) + \begin{pmatrix} \widetilde{M}(n,k_\parallel) & \widetilde{A}k_+ & 0 & 0 \\ \widetilde{A}k_- & -\widetilde{M}(n,k_\parallel) & 0 & 0 \\ 0 & 0 & \widetilde{M}(n,k_\parallel) & -\widetilde{A}k_- \\ 0 & 0 & -\widetilde{A}k_+ & -\widetilde{M}(n,k_\parallel) \end{pmatrix} \tag{S3}$$

where $k_\parallel = (k_x, k_y)$ and

$$\begin{aligned} \widetilde{\epsilon}_0(n,k_\parallel) =& \widetilde{C}_0 + \widetilde{C}_2(k_x^2+k_y^2) = [C_0 + C_1(n\pi/d)^2] + C_2(k_x^2+k_y^2) \\ \widetilde{M}(n,k_\parallel) =& \widetilde{M}_0 + \widetilde{M}_2(k_x^2+k_y^2) = [M_0 + M_1(n\pi/d)^2] + M_2(k_x^2+k_y^2) \end{aligned}$$

The parameters $C_0, C_1, C_2, M_0, M_1, M_2, A$ are assumed to remain the same as those in the effective $k\cdot p$ model for the germancite bulk in Eq. [S1]. If the low-energy electronic structure is dominated by four bands around the Fermi level, the effective model of the film can be further reduced to a four by four matrix. Bu generally, to correctly describe the low-energy states, the dimension of $H_d(k_\parallel)$ is higher than four and more than one indices n are included.

On the other hand, the topological phase transition is mainly determined by the lowest sub-bands around the Fermi level. And we find that the model Hamiltonian of these sub-bands $H_{n,d}$ shares the same from as the BHZ model [11]. According to the argument of BHZ, a topological phase transition can be induced when $\widetilde{M}_0\widetilde{M}_2$ changes its sign. In our system of germancite (111) film, $\widetilde{M}_2$ in the lowest sub-bands is positive and takes the same value as M_2 in Eq. [S1]. But $\widetilde{M}_0 = M_0 + M_1(n\pi/d)^2$, this term can change its sign with increasing film thickness and induce a topological phase transition. Consequently, the $\mathbb{Z}_2$ index of the film can change from 0 to 1 or vice versa. And we can infer that the germancite (111) film can be a quantum spin Hall insulator with proper thickness.

Moreover, since the bulk Dirac points are at $(0,0,\pm k_{z0})$, we have $M_0 + M_1 k_{z0}^2 = 0$ and $M_0 M_1 < 0$ according to the $k\cdot p$ model in Eq. [S1]. These are consistent with the fitting results of germancite and stancite in Table S1, where $M_0 < 0$ and $M_1 > 0$. Then the sign of $\widetilde{M}_0 = M_0 + M_1(n\pi/d)^2$ can change as the thickness d varies and the critical point is $d_c(n) = n\pi k_{z0}$. Therefore, as the thickness d increases, $\widetilde{M}_0\widetilde{M}_2$ changes its sign at each critical point $d_c(n)$, $n = 1, 2, 3, \cdots$. And whenever the sign change happens, there is a topological phase transition of the film.

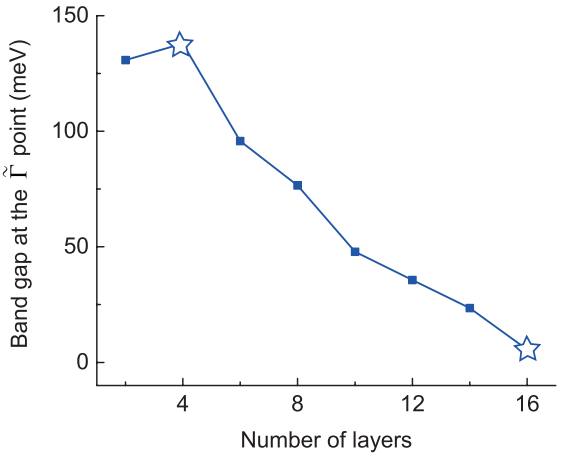

Supplementary Figure S2. The evolution of the band gap at the $\widetilde{\Gamma}$ point versus the number of layers of germancite (111) films. The basis states are the Wannier functions, which are constructed from the bulk *ab initio* calculations. The stars denote the cases where the band order at the $\widetilde{\Gamma}$ is topologically nontrivial.

Our numerical calculations of germancite (111) films with the Wannier functions are shown in Fig. S2. It can be seen that the band gap at the $\widetilde{\Gamma}$ point generally becomes smaller as the film gets thicker. When the film is thin enough (with about 2∼4 layers), the gap is relatively large due to the quantum confinement effect. With increasing thickness, the quantum confinement effect gets weaker and the gap generally decreases. This is because when the film is thick enough, the electronic structure of the film will converge to the 2D projection of the bulk states. More specifically, the 3D Dirac points will be projected onto the same $\widetilde{\Gamma}$ point in the 2D Brillouin zone and the film becomes gapless. The film with the thickness being 4-layer or 16-layer has a topologically nontrivial band order at the $\widetilde{\Gamma}$ point (see the stars). Thus, there are oscillations of the topological properties, which is consistent with the theoretical analysis above.

[1] Yang, B.-J. & Nagaosa, N. Classification of stable three-dimensional Dirac semimetals with nontrivial topology. *Nature Commun.* **5**, 4898 (2014).

[2] Fu, L. & Kane, C. L. Topological insulators with inversion symmetry. *Phys. Rev. B* **76**, 045302 (2007).

[3] Soluyanov, A. A. & Vanderbilt, D. Computing topological invariants without inversion symmetry. *Phys. Rev. B* **83**, 235401 (2011).

[4] Guloy, A. M. *et al.* A guest-free germanium clathrate. *Nature* **443**, 320 (2006).

[5] Kiefer, F. *et al.* Synthesis, structure, and electronic properties of 4*H*-germanium. *J. Mater. Chem.* **20**, 1780 (2010).

[6] Johnson, B. C. *et al.* Evidence for the **R**8 Phase of Germanium. *Phys. Rev. Lett.* **110**, 085502 (2013).

[7] Zhao, Z. *et al.* Tetragonal Allotrope of Group 14 Elements. *J. Am. Chem. Soc.* **134**, 12362 (2012).

[8] Ceylan, A., Gumrukcu, A. E., Akin, N., Ozcan, S. & Ozcelik, S. Formation of ST12 phase Ge nanoparticles in ZnO thin films. *Mater. Sci. Semicond. Process.* **40**, 407 (2015).

[9] Menoni, C. S., Hu, J. Z. & Spain, I. L. Germanium at high pressures. *Phys. Rev. B* **34**, 362 (1986)Phys. Rev. B 81, 041307(R) (2010) .

[10] Liu, C.-X., Zhang, H.-J., Yan, B., Qi, X.-L., Frauenheim, T., Dai, X., Fang, Z., & Zhang, S.-C. Oscillatory crossover from two-dimensional to three-dimensional topological insulators. *Phys. Rev. B* **81**, 041307(R) (2010).

[11] Bernevig, B. A., Taylor L., H. & Zhang, S.-C. Quantum Spin Hall Effect and Topological Phase Transition in HgTe Quantum Wells. *Science* **314**, 1757 (2006).